Table 4 | Top 5 canonical pathways predicted by an IPA analysis of miRNA targets

Ingenuity Canonical Pathways	-log(p-value)	Ratio	Molecules
Protein Kinase A Signaling	1.60E+00	2.46E-02	PDE2A,NFAT5,FLNA,DUSP1,GNG2,CHP1,ELK1,PTPN12,CDC25A,PDE1C
Calcium Signaling	1.54E+00	2.76E-02	NFAT5,CHRFAM7A,CHP1,CHRNA7,TPM4,TRPC3
Relaxin Signaling	1.50E+00	3.05E-02	PDE2A,GNAO1,GNG2,ELK1,PDE1C
Clathrin-mediated Endocytosis Signaling	1.49E+00	3.03E-02	SNX9,RAB5A,USP9X,CHP1,NUMB,MYO1E
Role of CHK Proteins in Cell Cycle Checkpoint Control	1.47E+00	5.08E-02	PPM1J,CDKN1A,CDC25A

Pattela classification confirmed in at least two visual field examinations, open anterior-chamber angles on gonioscopy, and elevated intraocular pressure (intraocular pressure (IOP) > 21 mm Hg by the Goldmann applanation tonometer); (2) The diagnosis criteria for NTG were identical to those for POAG, except that the IOP never exceeded 21 mm Hg; (3) PACG was defined as glaucomatous optic neuropathy, above characteristic visual field defect, and an occludible angle; (4) Pseudoexfoliation glaucoma (PEX) was defined in this study as glaucomatous optic neuropathy with the same characteristic visual field defects as the previously mentioned forms of glaucoma, an open anterior chamber angle in a gonioscopic examination, and the finding of characteristic exfoliative material on the anterior lens surface and/or in the iris in a slit-lamp examination, in one or both eyes. The presence of abnormal visual field defects meant that the results of a glaucoma hemifield test were outside normal limits and that a cluster of three or more nonedge points were present, all depressed on the pattern deviation plot at $P < 0.05$ (with one depressed at $P < 0.01$), as well as that the corrected pattern SD was significant at $P < 0.05$. An occludible angle was classified when the posterior trabecular meshwork could not be seen over an angle of 180 degrees or more without indentation.

Cataract and macular disorders such ERM are the most common non-exudative retinal diseases used as control groups in clinical ophthalmological studies, including those of glaucoma[44]. The eyes with ERM included in this study were exclusively eyes with idiopathic ERM, and did not have any other macular abnormalities. Eyes with secondary ERM (e.g., attributable to diabetic retinopathy, venous occlusion, retinal detachment, uveitis, or trauma) were thus excluded.

AH was collected from patients who met the inclusion criterion of having had no history of cancer, asthma, and ocular diseases other than glaucoma, cataract, and epiretinal membrane.

AH sampling and RNA isolation. Approximately 100 μl of AH was collected from each patient by anterior chamber paracentesis, using a 30-gauge needle inserted through the peripheral cornea at the beginning of the procedure. The needle did not contact any iris or lens tissue during the sample collection. AH was transferred to 1.5 ml siliconized tubes and immediately placed on ice. Samples were subsequently centrifuged for 10 min at 300 g for removing cellular components, and its aqueous phase was gently collected. The AH was mixed with 700 μl QIAzol Lysis reagent and stored at −80°C until further processing. Purification of miRNA from thawed AH/QIAzol samples were performed with miRNeasy Mini Kit (Qiagen, Valencia, CA). And fraction of small RNAs (<200 nucleotides) was conformed by Agilent 2100 bioanalyzer (Agilent teqnology) with a RNA 6000 Pico kit.

miRNA array preparation and analysis. MiRNA in purified RNA was measured using the Toray Industries miRNA analysis system, in which AH miRNA samples were hybridized to 3D-Gene human miRNA ver. 1.60 chips containing 2019 miRNAs (Toray Industries, Inc., Tokyo, Japan). MiRNA gene expression data were scaled by global normalization, and differential expression was analyzed[45]. Two-tailed, Welch's t-test was used to detect significant associations. P-values were adjusted for multiple testing based on the false discovery rate with the Bioconductor package q-value[46].

Bioinformatical analysis. After a determination was made of which miRNAs had significantly different levels of expression in the control subjects and glaucoma patients, the molecular targets of these miRNAs were predicted with DIANA-microT v3.0 (http://diana.cslab.ece.ntua.gr/microT/)[47]. Pathway and global functional analyses were performed with IPA software[48,49]. The dataset uploaded to the IPA application was the list of target molecules with miTG scores > 0.97000 from the DIANA-microT prediction. Values of plus one and minus one were assigned to the molecules predicted to be targeted by down- and up- regulated miRNAs, respectively.

1. Weiland, M., Gao, X. H., Zhou, L. & Mi, Q. S. Small RNAs have a large impact: circulating microRNAs as biomarkers for human diseases. *RNA Biol.* **9**, 850–859 (2012).
2. Lee, R. C., Feinbaum, R. L. & Ambros, V. The C. elegans heterochronic gene lin-4 encodes small RNAs with antisense complementarity to lin-14. *Cell.* **75**, 843–854 (1993).
3. Wightman, B., Ha, I. & Ruvkun, G. Posttranscriptional regulation of the heterochronic gene lin-14 by lin-4 mediates temporal pattern formation in C. elegans. *Cell.* **75**, 855–862 (1993).
4. Ouellet, D. L., Perron, M. P., Gobeil, L. A., Plante, P. & Provost, P. MicroRNAs in gene regulation: when the smallest governs it all. *J Biomed Biotech.* **2006**, 69616 (2006).
5. Filipowicz, W., Bhattacharyya, S. N. & Sonenberg, N. Mechanisms of post-transcriptional regulation by microRNAs: are the answers in sight? *Nat Rev Genet.* **9**, 102–114 (2008).
6. Belevych, A. E. *et al.* MicroRNA-1 and -133 increase arrhythmogenesis in heart failure by dissociating phosphatase activity from RyR2 complex. *PLoS One.* **6**, e28324 (2011).
7. Lu, J. *et al.* MicroRNA expression profiles classify human cancers. *Nature.* **435**, 834–883 (2005).
8. Baker, M. RNA interference: MicroRNAs as biomarkers. *Nature.* **464**, 1227 (2010).
9. Ju, J. miRNAs as biomarkers in colorectal cancer diagnosis and prognosis. *Bioanalysis.* **2**, 901–906 (2010).
10. Kosaka, N., Izumi, H., Sekine, K. & Ochiya, T. microRNA as a new immune-regulatory agent in breast milk. *Silence.* **1**, 7 (2010).
11. Weber, J. A. *et al.* The microRNA spectrum in 12 body fluids. *Clin Chem.* **56**, 1733–1741 (2010).
12. Zubakov, D. *et al.* MicroRNA markers for forensic body fluid identification obtained from microarray screening and quantitative RT-PCR confirmation. *Int J Legal Med.* **124**, 217–226 (2010).
13. Cortez, M. A. *et al.* MicroRNAs in body fluids--the mix of hormones and biomarkers. *Nat Rev Clin Oncol.* **8**, 467–477 (2011).
14. Dunmire, J. J., Lagouros, E., Bouhenni, R. A., Jones, M. & Edward, D. P. MicroRNA in aqueous humor from patients with cataract. *Exp Eye Res* **108**, 68–71 (2013).
15. Ragusa, M. *et al.* MicroRNAs in vitreus humor from patients with ocular diseases. *Mol Vis* **19**, 430–440 (2013).
16. Richardson, M. R. *et al.* Alterations in the aqueous humor proteome in patients with Fuchs endothelial corneal dystrophy. *Mol Vis.* **16**, 2376–2383 (2010).
17. Kunikata, H. *et al.* Intraocular concentrations of cytokines and chemokines in rhegmatogenous retinal detachment and the effect of intravitreal triamcinolone acetonide. *Am J Ophthalmol.* **155**, 1028–1037 (2013).
18. Duan, X. *et al.* Proteomic analysis of aqueous humor from patients with myopia. *Mol Vis.* **14**, 370–377 (2008).
19. Bouhenni, R. A. *et al.* Identification of differentially expressed proteins in the aqueous humor of primary congenital glaucoma. *Exp Eye Res.* **92**, 67–75 (2011).
20. Inoue, T., Kawaji, T. & Tanihara, H. Elevated levels of multiple biomarkers of Alzheimer's disease in the aqueous humor of eyes with open-angle glaucoma. *Invest Ophthalmol Vis Sci.* **54**, 5353–5358 (2013).
21. Janciauskiene, S., Westin, K., Grip, O. & Krakau, T. Detection of Alzheimer peptides and chemokines in the aqueous humor. *Eur J Ophthalmol.* **21**, 104–111 (2011).
22. Quigley, H. A. Number of people with glaucoma worldwide. *Br J Ophthalmol.* **80**, 389–393 (1996).
23. Quigley, H. A. & Broman, A. T. The number of people with glaucoma worldwide in 2010 and 2020. *Br J Ophthalmol.* **90**, 262–267 (2006).
24. Resnikoff, S. *et al.* Global data on visual impairment in the year 2002. *Bull World Health Organ.* **82**, 844–851 (2004).
25. Coca-Prados, M. & Escribano, J. New perspectives in aqueous humor secretion and in glaucoma: the ciliary body as a multifunctional neuroendocrine gland. *Prog Retin Eye Res.* **26**, 239–262 (2007).
26. Luna, C., Li, G., Qiu, J., Epstein, D. L. & Gonzalez, P. Role of miR-29b on the regulation of the extracellular matrix in human trabecular meshwork cells under chronic oxidative stress. *Mol Vis.* **28**, 2488–2497 (2009).
27. Luna, C., Li, G., Qiu, J., Epstein, D. L. & Gonzalez, P. Cross-talk between miR-29 and transforming growth factor-betas in trabecular meshwork cells. *Invest Ophthalmol Vis Sci.* **52**, 3567–3572 (2011).
28. Kawaji, H. & Hayashizaki, Y. Exploration of small RNAs. *PLoS Genet.* **4**, e22 (2008).
29. Vithana, E. N. *et al.* Collagen-related genes influence the glaucoma risk factor, central corneal thickness. *Hum Mol Genet.* **20**, 649–658 (2011).
30. Jaimes, M., Rivera-Parra, D., Miranda-Duarte, A., Valdés, G. & Zenteno, J. C. Prevalence of high-risk alleles in the LOXL1 gene and its association with pseudoexfoliation syndrome and exfoliation glaucoma in a Latin American population. *Ophthalmic Genet.* **33**, 12–17 (2012).

31. Burdon, K. P. *et al.* Glaucoma risk alleles at CDKN2B-AS1 are associated with lower intraocular pressure, normal-tension glaucoma, and advanced glaucoma. *Ophthalmol.* **119**, 1539–1545 (2012).
32. Carbone, M. A. *et al.* Genes of the unfolded protein response pathway harbor risk alleles for primary open angle glaucoma. *PLoS One.* **6**, e20649 (2011).
33. Primus, S., Harris, A., Siesky, B. A. & Guidoboni, G. Diabetes: a risk factor for glaucoma? *Br J Ophthalmol.* **95**, 1621–1622 (2011).
34. Marcus, M. W., de Vries, M. M., Junoy Montolio, F. G. & Jansonius, N. M. Myopia as a risk factor for open-angle glaucoma: a systematic review and meta-analysis. *Ophthalmol.* **118**,1989–1994 (2011).
35. Marcus, D. M. *et al.* Sleep disorders: a risk factor for normal-tension glaucoma? *J Glaucoma.* **10**, 177–183 (2001).
36. Peng, C. H. *et al.* MicroRNAs and cataracts: correlation among let-7 expression, age and the severity of lens opacity. *Br J Ophthalmol.* **96**, 747–751 (2012).
37. Mu, G. *et al.* Correlation of overexpression of HMGA1 and HMGA2 with poor tumor differentiation, invasion, and proliferation associated with let-7 down-regulation in retinoblastomas. *Hum Pathol.* **41**, 493–502 (2010).
38. Libby, R. T. *et al.* Susceptibility to neurodegeneration in a glaucoma is modified by Bax gene dosage. *PloS Genet.* **1**, 17–26 (2005).
39. Vajaranant, T. S. & Pasquale, L. R. Estrogen deficiency accelerates aging of the optic nerve. *Menopause.* **19**, 942–947 (2012).
40. Fu, C. T., Tran, T. & Sretavan, D. Axonal/glial upregulation of EphB/ephrin-B signaling in mouse experimental ocular hypertension. *Invest Ophthalmol Vis Sci.* **51**, 991–1001 (2010).
41. Kawano, M., Kawaji, H., Grandjean, V., Kiani, J. & Rassoulzadegan, M. Novel small noncoding RNAs in mouse spermatozoa, zygotes and early embryos. *PLoS One.* **7**, e44542 (2012).
42. Kawaji, H. *et al.* The FANTOM web resource: from mammalian transcriptional landscape to its dynamic regulation. *Genome Biol.* **10**, R40 (2009).
43. Severin, J. *et al.* FANTOM4 EdgeExpressDB: an integrated database of promoters, genes, microRNAs, expression dynamics and regulatory interactions. *Genome Biol.* **10**, R39 (2009).
44. Honkanen, R. A. *et al.* Vitreous amino acid concentrations in patients with glaucoma undergoing vitrectomy. *Arch Ophthalmol.* **121**, 183–188 (2003).
45. Ohno, M. *et al.* The flavonoid apigenin improves glucose tolerance through inhibition of microRNA maturation in miRNA103 transgenic mice. *Sci Rep.* **3**, 2553 (2013).
46. John, D. S., Robert, T. *et al.* Statistical significance for genomewide studies. *Proc Natl Acad Sci USA.* **100**, 9440–9445 (2003).
47. Maragkakis, M. *et al.* Accurate microRNA target prediction correlates with protein repression levels. *BMC Bioinformatics.* **10**, 295 (2009).
48. Ramayo-Caldas, Y. *et al.* Liver transcriptome profile in pigs with extreme phenotypes of intramuscular fatty acid composition. *BMC Genomics.* **13**, 547 (2012).
49. Prat-Vidal, C. *et al.* Identification of temporal and region-specific myocardial gene expression patterns in response to infarction in swine. *PLoS One* **8**, e54785 (2013).

Acknowledgments

We thank the patients and medical staff from Tohoku university Hospital for their kind cooperation in this study. This study was supported by Leave a Nest - TORAY Industries award (Y.T.), Grants-in-Aid from the Ministry of Education, Science and Technology of Japan (24659756 for T.N., and 40625513 and 26670263 for Y.T.), and donative funds from Senju Pharmaceutical Co., Ltd and NIDEK Co., Ltd.

Author contributions

Y.T. designed the research. H.K. and T.N. sampled the aqueous humor from the patients. Y.T. and J.S. analyzed the aqueous humor samples with the microarray system. Y.T., S.T., T.K., M.Y., K.M.N. and T.I. analyzed the data thus obtained. Y.T. prepared the manuscript.

Additional information

Supplementary information accompanies this paper at http://www.nature.com/scientificreports

Competing financial interests: The authors declare no competing financial interests.

How to cite this article: Tanaka, Y. *et al.* Profiles of Extracellular miRNAs in the Aqueous Humor of Glaucoma Patients Assessed with a Microarray System. *Sci. Rep.* **4**, 5089; DOI:10.1038/srep05089 (2014).

BRAIN RESEARCH 1586 (2014) 203–212

Available online at www.sciencedirect.com

ScienceDirect

www.elsevier.com/locate/brainres

Brain Research

Research Report

Neuroprotective effect against axonal damage-induced retinal ganglion cell death in apolipoprotein E-deficient mice through the suppression of kainate receptor signaling

Kazuko Omodaka[a], *Koji M. Nishiguchi*[a], *Masayuki Yasuda*[a], *Yuji Tanaka*[a], *Kota Sato*[a], *Orie Nakamura*[a], *Kazuichi Maruyama*[a], *Toru Nakazawa*[a,b,c,*]

[a]*Department of Ophthalmology and Visual Science, Tohoku University Graduate School of Medicine, Sendai, Miyagi, Japan*

[b]*Department of Advanced Ophthalmic Medicine, Tohoku University Graduate School of Medicine, Sendai, Miyagi, Japan*

[c]*Department of Retinal Disease Control, Tohoku University Graduate School of Medicine, Sendai, Miyagi, Japan*

ARTICLE INFO

Article history:
Accepted 18 August 2014
Available online 24 August 2014

Keywords:
Glaucoma
Retinal ganglion cell
Optic nerve
Astrocyte
Excitotoxicity

ABSTRACT

Apolipoprotein E (ApoE) plays important roles in the body, including a carrier of cholesterols, an anti-oxidant, and a ligand for the low-density lipoprotein receptors. In the nervous system, the presence of ApoE4 isoforms is associated with Alzheimer's disease. ApoE gene polymorphisms are also associated with glaucoma, but the function of ApoE in the retina remains unclear. In this study, we investigated the role of ApoE in axonal damage-induced RGC death. ApoE was detected in the astrocytes and Müller cells in the wild-type (WT) retina. RGC damage was induced in adult ApoE-deficient mice (male, 10–12 weeks old) through ocular hypertension (OH), optic nerve crush (NC), or by administering kainic acid (KA) intravitreally. The WT mice were treated with a glutamate receptor antagonist (MK801 or CNQX) 30 min before performing NC or left untreated. Seven days later, the retinas were flat mounted and Fluorogold-labeled RGCs were counted. We found that the RGCs in the ApoE-deficient mice were resistant to OH-induced RGC death and optic nerve degeneration 4 weeks after induction. In WT mice, NC effectively induced RGC death (control: 4085 ± 331 cells/mm^2, NC: 1728 ± 170 cells/mm^2). CNQX, an inhibitor of KA receptors, suppressed this RGC death (3031 ± 246 cells/mm^2), but MK801, an inhibitor of NMDA receptors, did not (1769 ± 212 cells/mm^2). This indicated the involvement of KA receptor signaling in NC-induced RGC death. We found that NC- or KA-induced RGC death

Abbreviations: ApoE, Apolipoprotein E; NC, nerve crush; KA, kainic acid; WT, wild-type; IOP, intraocular pressure; POAG, primary open angle glaucoma; NTG, normal tension glaucoma; RGCs, retinal ganglion cells; LDL, low density lipoprotein; OH, ocular hypertension; IHC, immunohistochemistry; INL, inner nuclear layer; GCL, ganglion cell layer; IPL, inner plexiform layer; OPL, outer plexiform layer; ONL, outer nuclear layer

*Corresponding author at: Tohoku University Graduate School of Medicine, Department of Ophthalmology, 1-1 Seiryo, Aoba, Sendai, Miyagi 980-8574, Japan. Fax: +81 22 717 7298.
E-mail address: ntoru@oph.med.tohoku.ac.jp (T. Nakazawa).

http://dx.doi.org/10.1016/j.brainres.2014.08.053

was significantly less in the ApoE-deficient mice than in the WT mice. These data suggest that the ApoE deficiency had a neuroprotective effect against axonal damage-induced RGC death by suppressing the KA receptor signaling.

1. Introduction

Glaucoma is a complex, heterogeneous disease characterized by the progressive degeneration of the axons of the optic nerve. It is the second most common cause of blindness worldwide, affecting approximately 70 million people (Quigley, 1996; Resnikoff et al., 2004; Weinreb and Khaw, 2004). The primary symptom of glaucoma is progressive loss of the visual field, characterized by visual field defects corresponding to thinning of the neuronal rim of the optic nerve head. Treatments for glaucoma aim to delay this progressive loss and prevent the deterioration of patients' quality of life. Elevated intraocular pressure (IOP) is widely recognized as a major risk factor for glaucoma, and lowering IOP is well established as a glaucoma treatment. IOP-lowering treatment is used not only for primary open angle glaucoma (POAG), but also for normal tension glaucoma (NTG), in which IOP remains within normal bounds (Collaborative Normal-Tension Glaucoma Study Group, 1998; Heijl et al., 2002). Significant risk factors for NTG, the major type of glaucoma in Asia (Iwase et al., 2004; Kim et al., 2011; Liang et al., 2011), include myopia, aging, and high IOP (Suzuki et al., 2006). In the clinical treatment of glaucoma, a variety of eye drops are used to lower IOP. Although evidence shows that lowering IOP is effective, NTG is believed to be multifactorial, arising from the interaction of many endogenous, environmental, and genetic factors. Despite its complicated pathogenesis, it is clear that the retinal ganglion cells (RGCs) are particularly vulnerable in the process of glaucomatous degeneration. Neuroprotection against RGC death has thus been emphasized as an important goal in disease management (Levin, 2003), though effective treatments have yet to be found.

Epidemiological studies are a promising source of new approaches to glaucoma research that may clarify the pathogenesis of glaucoma. Recently, population-based research has suggested that the long-term use of statins, e.g., HMG-CoA reductase inhibitors, appears to be associated with a reduced risk of OAG. Moreover, the observed effects were independent of IOP (Marcus et al., 2012) and included the suppression of glaucoma progression (De Castro et al., 2007). These findings have led to greater emphasis on lipid metabolism as a focus of glaucoma research. A number of groups, including ours, have previously demonstrated that statins have a neuroprotective effect against damage to the retinal neurons during ischemia-reperfusion injury (Honjo et al., 2002; Kawaji et al., 2007) and excitotoxicity-induced retinal cell death, and that this protection acts via an anti-inflammatory effect (Nakazawa et al., 2007b). However, HMG-CoA reductase is not effective at lowering cholesterol in rodents, and the neuroprotective effects of statins are unrelated to cholesterol levels.

Apolipoprotein E (ApoE) plays a key role in the human body as a carrier of cholesterol (Mahley, 1988). In the central nervous system, the main sources of ApoE synthesis are the astrocytes and microglia. Secreted ApoE binds to cholesterols, and the resulting ApoE–cholesterol complex is internalized into the RGCs through the low density lipoprotein (LDL) receptors before being transferred to the optic nerve (Amaratunga et al., 1996). ApoE also has multipotential effects on the pathologies underlying Alzheimer's disease, including anti-inflammatory, synapse repair and plasticity, and anti-oxidant effects (Bu, 2009). ApoE has 3 subtypes: E2, E3, and E4. The frequency of ApoE4 is significantly higher in Alzheimer's disease, and glaucoma patients have also been found to have a higher frequency of ApoE4 than age-matched controls (Tamura et al., 2006). E4 has less potential as an anti-inflammatory and anti-oxidant (Bu, 2009). Single nucleotide polymorphisms (SNPs) in ApoE are associated with both POAG and NTG (Lam et al., 2006; Mabuchi et al., 2005; Ressiniotis et al., 2004; Zetterberg et al., 2007). These previous findings prompted the present investigation of ApoE's role in the mechanism of RGC death in glaucoma.

In this study, we first investigated the distribution of ApoE in adult mouse retinas and the involvement of ApoE in a mouse model of ocular hypertension (OH)-induced RGC death, using wild-type (WT) mice and ApoE$^{-/-}$ mice. Next, we examined how ApoE deficiency affected the cytotoxic effects that occur in nerve crush (NC)- and excitotoxicity-induced RGC death. We found that ApoE deficiency had a neuroprotective effect. In the ApoE$^{-/-}$ mice, this was achieved through the suppression of kainic acid (KA) receptor signaling. Thus, we are able to report important new information that will affect future strategies for the development of neuroprotective treatments for glaucoma.

2. Results

2.1. *Distribution of ApoE in the retina and optic nerve*

We investigated the distribution of ApoE in the retina and optic nerve with immunohistochemistry (IHC; $n=4$). Immunoreactivity for ApoE was detected in the inner margin of the retina, the spindle-shaped cells in the inner nuclear layer (INL) (Fig. 1A,E) and was ubiquitous in the optic nerve (Fig. 1I). Double IHC showed that in the retina, ApoE was localized in the Müller cells (Fig. 1B) and the astrocytes (Fig. 1F), and in the optic nerve, it was localized in the astrocytes (Fig. 1J). Interestingly, examining the cellular distribution of ApoE revealed that it was also present in the cytosol of the astrocytes.

2.2. *Ocular hypertension damage in ApoE$^{-/-}$ mice*

To investigate the role of ApoE in OH, elevated IOP was induced in the ApoE$^{-/-}$ and WT mice. IOP was then measured

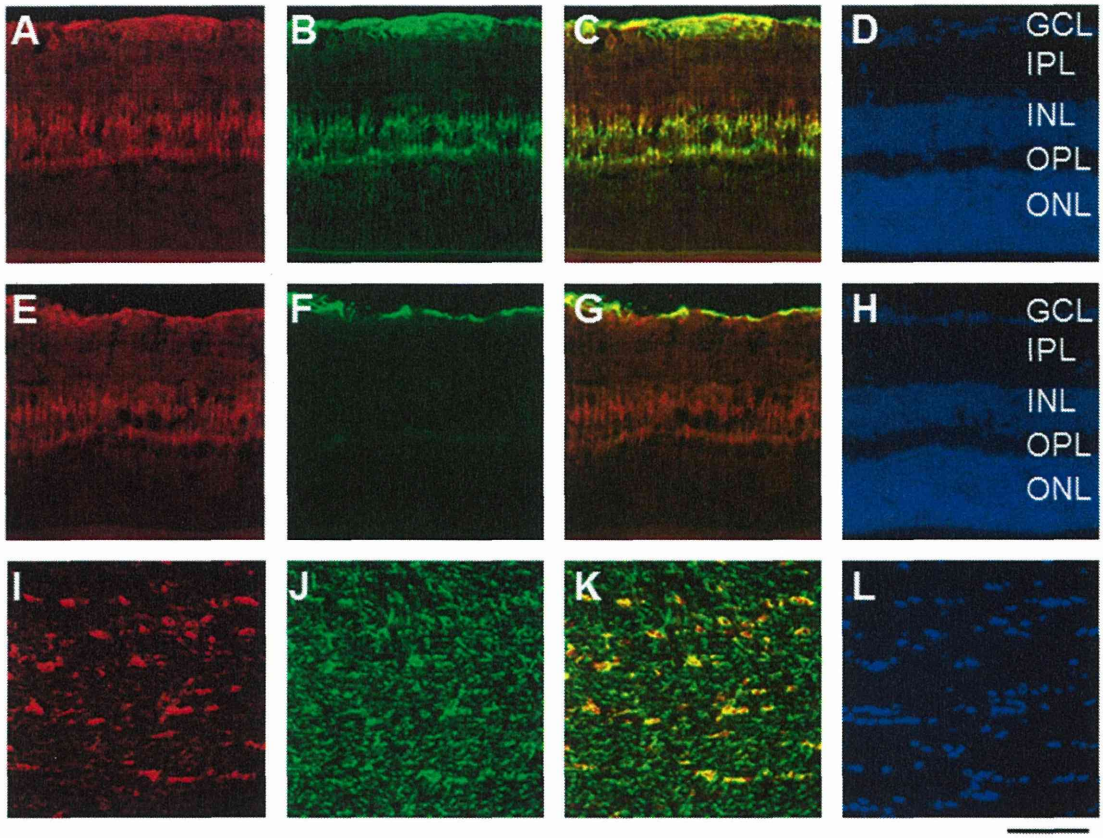

Fig. 1 – Immunohistochemical staining with an ApoE antibody and a retinal glial cell marker in the retina and optic nerve of adult mice. (A–D) Double staining with ApoE and glutamine synthetase as a marker of Müller cells in the retina. (A) Immunoreactivity (IR) of ApoE. (B) IR of glutamine synthetase. (C) Merged image. (D) DAPI nuclear staining. Note that the IR of ApoE and glutamine synthetase were localized. (E–H) Double staining with ApoE and GFAP as a marker of astrocytes in the retina. (E) IR of ApoE. (F) IR of GFAP. (G) Merged image. (H) DAPI nuclear staining. Note that the IR of ApoE and GFAP were localized. (I–L) Double staining with ApoE and GFAP as a marker of astrocytes in transverse sections of the optic nerve. (I) IR of ApoE. (J) IR of GFAP. (K) Merged image. (L) DAPI nuclear staining. Note that the IR of ApoE and GFAP was localized in the optic nerve. GCL: ganglion cell layer, IPL: inner plexiform layer, INL: inner nuclear layer, OPL: outer plexiform layer, ONL: outer nuclear layer. Scale bar, 100 μm.

over the course of 4 weeks, as previously described (Nakazawa et al., 2006). Laser photocoagulation blocks the normal flow of aqueous humor, and in this study was able to increase IOP by approximately 100% over its baseline value (14 mmHg) between the first and the fourth weeks. In wild-type mice, the average IOP in the laser-treated eyes was 16.4 mmHg (control), 32.6 mmHg (1 week), 31.0 mmHg (2 weeks), 31.5 mmHg (3 weeks), and 29.5 mmHg (4 weeks). In the ApoE-deficient mice, the average IOP in the laser-treated eyes was 15.9 mmHg (control), 31.7 mmHg (1 week), 32.6 mmHg (2 weeks), 30.8 mmHg (3 weeks), and 31.1 mmHg (4 weeks). There were no differences between ApoE$^{-/-}$ mice and WT mice (Fig. 2). Three weeks after the induction of OH, the density of Di-I-labeled RGCs decreased significantly in the WT mice, and by the fourth week the RGCs had decreased by 30%. By contrast, there was no detectible decrease in the density of Di-I-labeled RGCs in the ApoE$^{-/-}$ mice ($n=8$, Fig. 3). Next, we investigated the specific role of ApoE in axonal damage after OH induction. Phosphorylated neurofilaments are considered to reflect the integrity of the axons as dephosphorylation of the neurofilaments leads to destabilization of the axon filaments in OH-induced axonal degeneration (Kashiwagi et al., 2003). Four weeks after OH induction, the immunoreactivity of phosphorylated NFs (SMI-31R) decreased in the WT mice (Fig. 4). Consistent with this decrease in phosphorylated NFs, decreased axon density was detected after 2 weeks, becoming significant at 3 weeks ($n=8$, $p<0.01$) and 4 weeks ($n=8$, $p<0.01$) (Fig. 4). On the other hand, the decrease in the immunoreactivity of SMI-31R and the density of the axons was only minor in the ApoE$^{-/-}$ mice (Fig. 4).

2.3. *The susceptibility of ApoE$^{-/-}$ mice to NC-induced RGC death*

To investigate whether ApoE played a role in NC-induced RGC death, we performed NC in both ApoE$^{-/-}$ and WT mice and assessed the density of FG-labeled surviving RGCs. Before NC, there was no difference in RGC density between the WT (4085.4±331.0 cells/mm^2) and ApoE$^{-/-}$ mice (4221.5± 513.9 cells/mm^2). Seven days after NC, the RGC density was

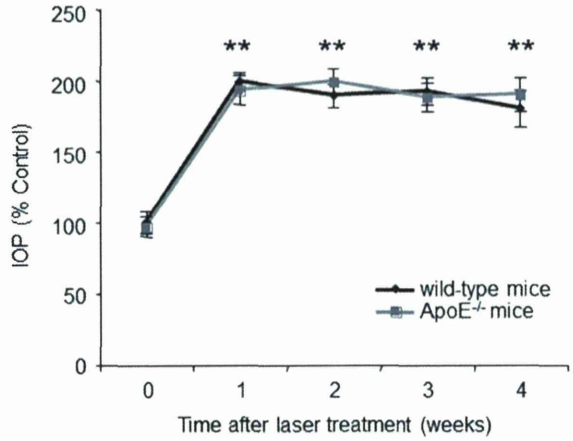

Fig. 2 – Time course of IOP change after laser-induced ocular hypertension ($n=8$) both in wild-type and ApoE$^{-/-}$ mice. IOP was measured at the indicated time points using an applanation tonometer. Data express % vs. control. There were no differences between the wild-type and ApoE$^{-/-}$ mice. **P < 0.01 compared to control.

significantly lower in the WT mice than in the ApoE$^{-/-}$ mice (1728.4 ± 170.6 cells/mm^2 and 2562.7 ± 141.0 cells/mm^2, respectively, p=0.034, Fig. 5). This neuroprotective effect of ApoE deficiency was still active 14 days after NC, with the WT mice still having a significantly lower density of surviving RGCs than the ApoE$^{-/-}$ mice (528.9 ± 125.4 cells/mm^2 and 1905.9 ± 238.5 cells/mm^2, respectively, $p=0.004$, Fig. 5).

2.4. *NC-induced RGC death through the kainite pathway in WT mice*

In rats, glutamate receptor signaling has been implicated in the NC-induced RGC death (Schmitt and Sabel, 1996; Schuettauf et al., 2000). To further investigate the mechanism of ApoE deficiency's neuroprotective effect in the RGCs, we performed NC in WT mice and simultaneously administered one of two glutamate receptor inhibitors, CNQX and MK801, or PBS. Seven days later, we found that CNQX, an inhibitor of KA receptors, had a significant neuroprotective effect against NC-induced RGC death (PBS: 1728.4 ± 170.6 cells/mm^2, CNQX: 3031.6 ± 246.9 cells/mm^2, $p=0.020$, Fig. 6), but MK801, an inhibitor of NMDA receptors, did not (1769.6 ± 211.9 cells/mm^2, $p=0.663$).

2.5. *Reduced susceptibility to KA toxicity in ApoE$^{-/-}$ mice*

To investigate the susceptibility of ApoE$^{-/-}$ mice to KA toxicity, we injected graded concentrations of KA (0.1, 1, and 10 nmol/eye) or a control (PBS) intravitreally and counted the density of FG-labeled RGCs in both WT and ApoE$^{-/-}$ mice after 7 days. There was no difference in the density of FG-labeled RGCs in the WT mice injected with PBS or 0.1 nmol/eye of KA. However, there was a significantly higher number of surviving RGCs in the ApoE$^{-/-}$ mice than the WT mice after we administered 1 nmol/eye of KA (WT mice: 2719.8 ± 204.9 cells/mm^2, ApoE$^{-/-}$ mice: 4279.2 ± 471.4 cells/mm^2, $p=0.004$) or 10 nmol/eye of KA (WT mice: 797.6 ± 109.1 cells/mm^2, ApoE$^{-/-}$ mice: 1363.3 ± 222.8 cells/mm^2, $p=0.021$; Fig. 7).

3. Discussion

Although ApoE is believed to contribute to the pathophysiology of glaucoma (Lam et al., 2006; Mabuchi et al., 2005; Ressiniotis et al., 2004; Zetterberg et al., 2007), its exact role remains unclear. In this study, we examined the distribution of ApoE and found that it was located in the astrocytes and Müller cells of the retina and in the astrocytes of the optic nerve (Fig. 1). We also found evidence that the RGCs in the ApoE-deficient mice were resistant to death induced by elevated IOP both in the retina (Fig. 2) and in the optic nerve (Fig. 3). To further investigate the mechanism of neuroprotection due to ApoE deficiency, we performed a NC procedure in ApoE-deficient and WT mice to direct our focus on the axonal injury that is believed to contribute to the RGC death in OH (Nakazawa et al., 2006). We found that the ApoE-deficient mice also had a significant resistance to NC-induced RGC death. In WT mice, RGC death following NC was mediated in part by the KA receptor signaling. Since the ApoE-deficient mice were also resistant to KA-induced excitotoxicity, it is probable that the lack of ApoE inhibited the KA receptor signaling. Thus, this is the first report to demonstrate the critical role of ApoE in axonal damage-induced RGC death in mice, and to show that the mechanism of this role probably involved the inhibition of the cytotoxic KA pathway.

In this study, we used laser-induced OH in mice as a model of glaucoma. Previously, the DBA/2J mouse line was established to have a spontaneous mutation that leads to glaucoma, and the use of these mice has contributed greatly to research in this field (Libby et al., 2005a). However, there are limitations to this model, including delayed RGC loss and a considerable inter-individual variability. Moreover, use of this mouse line precludes the use of genetically altered mice. On the other hand, a laser-induced OH model of glaucoma allows high IOP to be rapidly and reliably induced in genetically altered mice, key advantages for investigating the role of target genes (Nakazawa et al., 2006). Here, we found that both OH-induced axonal degeneration and cell body loss were mitigated in ApoE-deficient mice. Furthermore, previous research has shown that the loss of the RGC soma and the loss of the RGC axons have different mechanisms, and that Bax deficiency prevents the former but not the latter (Libby et al., 2005b). This implies that the neuroprotective effect of ApoE deficiency is related to both OH-induced axonal degeneration and RGC loss.

As glaucoma has heterogeneous risk factors, we have previously used several different methods to mimic the human pathogenesis of glaucoma in mice and investigate the mechanism of RGC death: induced OH (Nakazawa et al., 2006), NC (Himori et al., 2013), vinblastine-induced blockage of axoplasmic flow (Ryu et al., 2012), excitotoxicity (Nakazawa et al., 2007b), and hyperglycemia (Shanab et al., 2012). We reported that OH-induced axonal degeneration occurred in part through the up-regulation of TNFα and subsequent microglial activation (Nakazawa et al., 2006), and that axonal damage-induced RGC death was related to oxidative stress

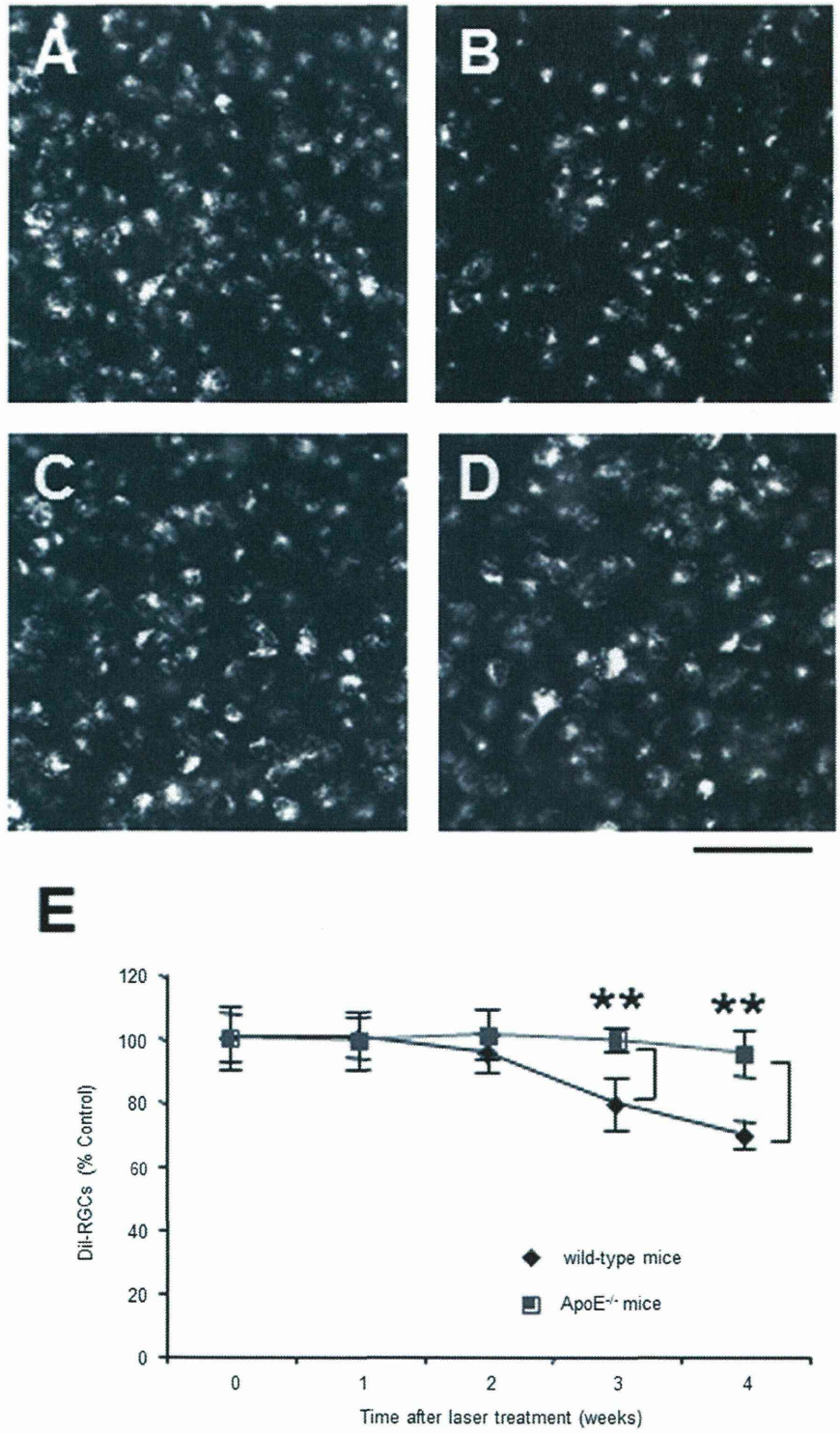

Fig. 3 – Time course of change in Di-I-labeled RGCs after laser-induced ocular hypertension in both wild-type and ApoE$^{-/-}$ mice (A-D) Representative photographs of Di-I-labeled RGCs in flat-mounted retinas (scale bar = 100 μm) 4 weeks after increasing IOP. (A, B) Wild-type mice. (C, D) ApoE$^{-/-}$ mice. (A, C) Control. (B, D) Ocular hypertension. (E) Quantification of Di-I-labeled RGCs in wild-type and ApoE$^{-/-}$ mice after increasing IOP. $^{**}P < 0.01$ compared to wild-type mice at the same time point ($n = 8$ per time point).

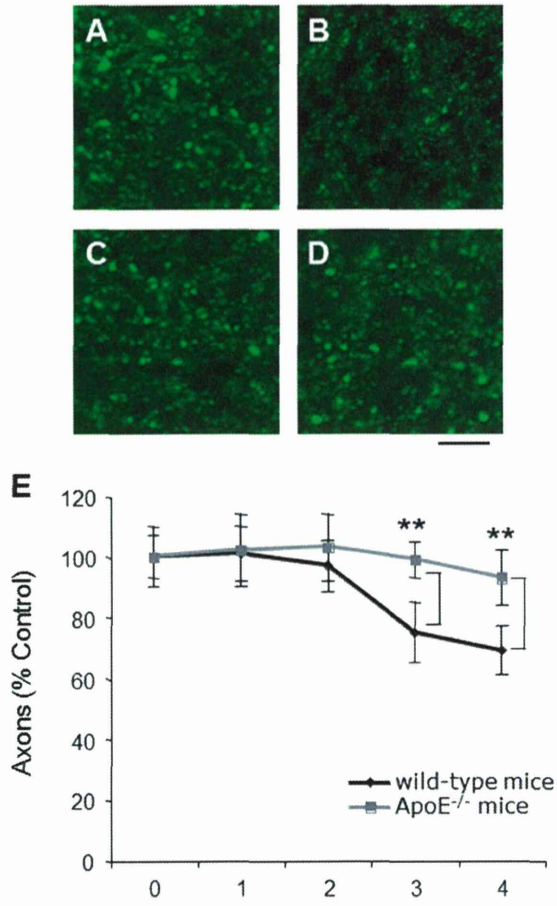

Fig. 4 – Time course of axonal degeneration after laser-induced ocular hypertension in both wild-type and ApoE$^{-/-}$ mice. (A–D) Representative photography showing the immunoreactivity of anti-phosphorylated neurofilaments in transverse sections of the optic nerve (scale bar = 10 μm) 4 weeks after increasing IOP. (A, B) Wild-type mice. (C, D) ApoE$^{-/-}$ mice. (A, C) Control. (B, D) Ocular hypertension. (E) Quantification of axon count in wild-type and ApoE$^{-/-}$ mice after increasing IOP. $^{**}P < 0.01$ compared to wild-type mice at the same time point ($n = 8$ per time point).

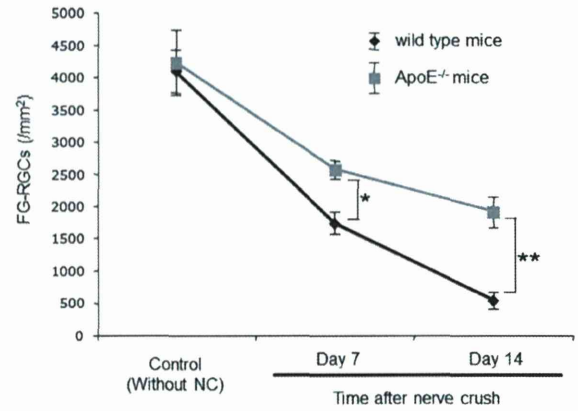

Fig. 5 – Time course of quantitative data for FG-labeled RGC death following nerve crush ($n = 8$ per time point) in both wild-type and ApoE$^{-/-}$ mice. $^{*}P < 0.05$ and $^{**}P < 0.01$ compared to wild-type mice at the same time point.

(Himori et al., 2013), calpain activation (Ryu et al., 2012), and endoplasmic reticulum stress (Yasuda et al., 2014). In the current study, both KA-induced excitotoxicity and NC-induced RGC death were ameliorated in ApoE-deficient mice. Notably, CNQX, an inhibitor of the KA receptors, suppressed NC-induced RGC loss, but a suppresser of the NMDA receptors did not. This indicates that KA-induced excitotoxicity was significantly involved in RGC death in these mouse models. However, the details of this mechanism remain unclear, and further study is needed to understand the degree of crosstalk that may occur between the ApoE and KA pathways.

IHC showed that ApoE was localized in the astrocytes of both the retinas and optic nerves of mature mice. During the development of the mouse retina, the postnatal switchover of lipoprotein from ApoA-I to ApoE has been reported to occur after around 5–7 days (Kurumada et al., 2007). Additionally, ApoE was found to be localized in the Golgi apparatus in the cytosol of the astrocytes that secrete it (Boyles et al., 1985; Kurumada et al., 2007). ApoE and its receptor, LDL receptor-related protein (LRP1), have also been implicated in cellular differentiation, neuroprotection, and axonal growth of the RGCs (Hayashi et al., 2004; Hayashi et al., 2007; Hayashi et al., 2009; Hayashi et al., 2012). Furthermore, the retinal glial cells from ApoE-deficient mice were found not to induce the axonal elongation of the RGCs in vitro (Hayashi et al., 2004). These findings suggest that glia-derived ApoE and the subsequent activation of LRP1 play an important role in the development of the RGCs. Furthermore, the retinal structure of ApoE-deficient mice becomes severely degraded 35 weeks after birth (Ong et al., 2001; Ong et al., 2003). We therefore used 12-week-old mice, as their retinal structure remains intact. Interestingly, damage to the glial cells specifically caused by gliotoxin has also been found lead to subsequent damage to the retinal structure in WT mice (Jablonski and Iannaccone, 2000). In the central nervous system, astrocyte-derived ApoE has been shown to regulate brain homeostasis (Gee and Keller, 2005). These findings suggest that glia-derived ApoE has various beneficial effects that help RGCs to survive in adult mice.

In this study, we found that ApoE deficiency had a neuroprotective effect against damage caused by insults to the retina. This beneficial effect of ApoE remains difficult to explain. With advanced age, the glial cells of ApoE-deficient mice also become significantly damaged (Ong et al., 2001; Ong et al., 2003). One possible explanation of the neuroprotective effect of ApoE deficiency in mice is thus dysfunction of the glial cells. In the pathogenesis of OH-, NC-, and excitotoxicity-induced RGC death, astrocytes play a cytotoxic role in the RGCs, involving TNFα (Nakazawa et al., 2006), nitric oxide (Morgan, 2000), matrix metalloproteinase-9 (Zhang et al., 2004), tissue plasminogen activators, and urokinase plasminogen activators (Ganesh and Chintala, 2011). Recent reports have suggested that endogenous ApoE is distributed in the caveolin-1-rich domain (membrane raft), where the various receptors are located and intracellular signaling starts, along with the ATP-binding cassette

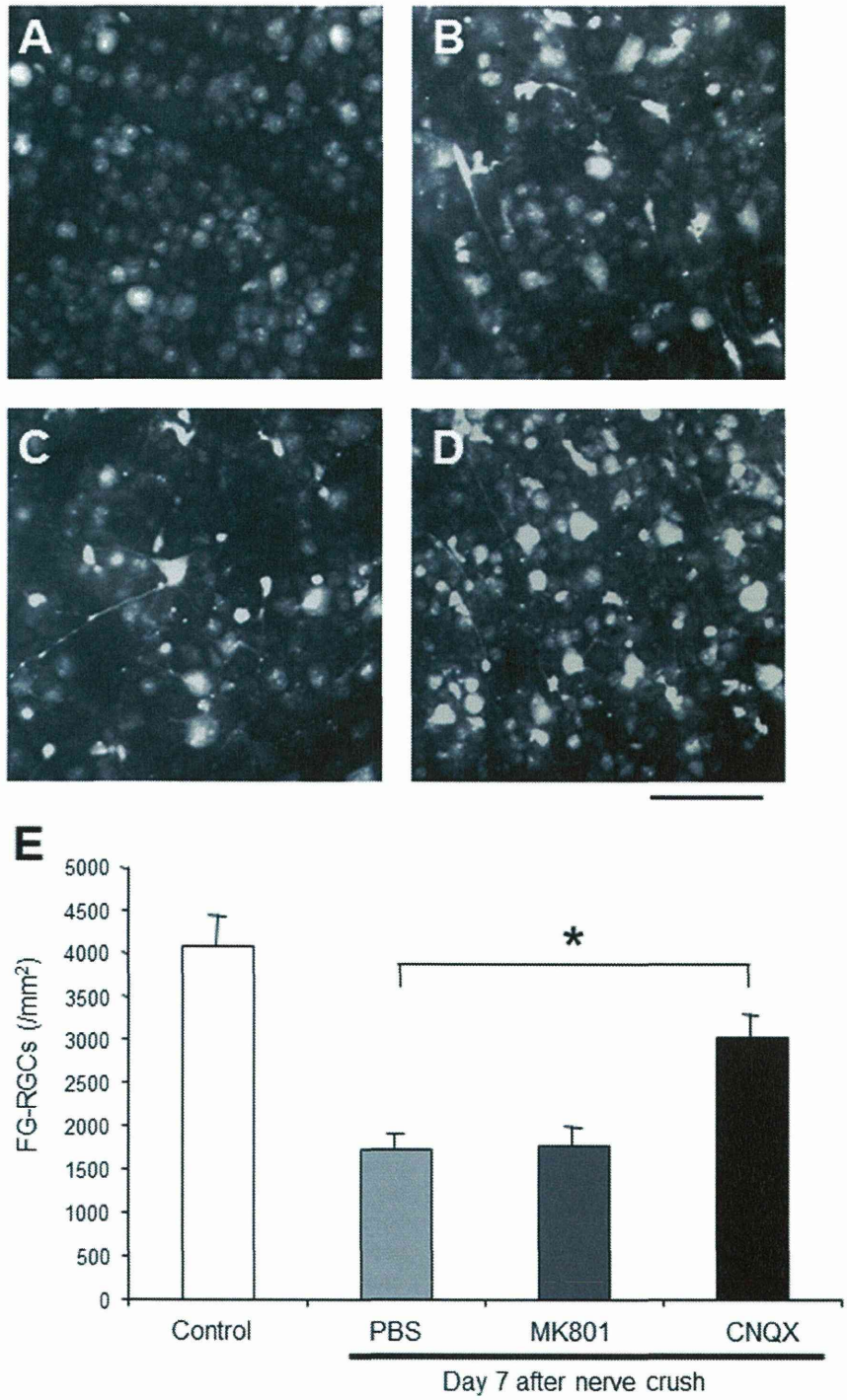

Fig. 6 – The neuroprotective effect of glutamate receptor antagonists in wild-type mice. (A-D) Representative photographs of FG-labeled RGCs in flat-mounted retinas (scale bar = 100 μm) 7 days after nerve crush. (A) Control. (B) PBS. (C) MK801. (D) CNQX. (E) Quantification of FG-labeled RGCs in wild-type mice 7 days after nerve crush. *$P < 0.05$ compared to PBS treatment.

transporter A1 in the astrocytes (Ito et al., 2014). Therefore, the dysfunction of glial cells induced by the deletion of ApoE, with its multipotential roles, may be related to the protective effect in damaged RGCs.

In conclusion, our studies in an experimental mouse model show that ApoE plays a critical role in the pathophysiological events that occur in ocular hypertension and after nerve crush. In ApoE-deficient mice, the cytotoxic pathways involving the KA receptors were suppressed. The blockade of KA-induced excitotoxicity, and possibly the upstream suppression of the astrocytes, may be an important future approach to the treatment of glaucoma.

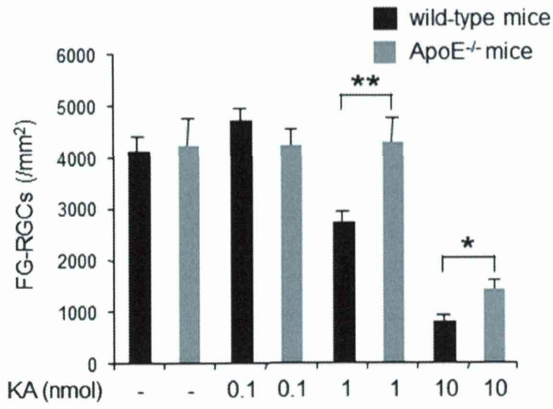

Fig. 7 – The neuroprotective effect of ApoE deficiency against KA-induced excitotoxicity in wild-type and ApoE$^{-/-}$ mice. Quantification of FG-labeled RGCs 7 days after nerve crush. *$P<0.05$ between wild-type and ApoE$^{-/-}$ mice with the same KA concentration ($n=8$ each).

4. Experimental procedure

4.1. Animals

In total, 124 male WT mice (C57BL/6, age 12 weeks, 23–27 g) and 96 ApoE$^{-/-}$ mice (age 12 weeks, 25–30 g) were used. All mice were maintained under a constant cycle of 12 h of light and 12 h of darkness in covered cages and were fed with a standard rodent diet ad libitum. The ApoE$^{-/-}$ mice were purchased from the Jackson Laboratory (Bar Harbor, ME). All animals were maintained and handled in accordance with the principles presented in the Guidelines for the Use of Animals in Neuroscience Research and the guidelines from the Declaration of Helsinki and the Guiding Principles in the Care and Use of Animals. The right eye of each animal was used as the experimental eye and the left eye served as a control. The surgical procedures were performed under deep anesthesia induced with the intramuscular administration of a mixture of ketamine (100 mg/kg, Phoenix Scientific, Inc., St. Joseph, MO) and xylazine (10 mg/kg, Phoenix Scientific, Inc.). All mice were euthanatized with an intraperitoneal injection of a lethal dose of pentobarbital.

All experimental procedures described in the present study were judged to meet the standards of the Association for Research in Vision and Ophthalmology Statement for the Use of Animals in Ophthalmic and Vision Research and used a protocol approved by the Animal Care Committee of the Ethics Committee for Animal Experiments at Tohoku University Graduate School of Medicine. All animals were treated according to the National Institutes of Health guidelines for the care and use of laboratory animals.

4.2. *Surgical procedure for retrograde labeling and RGC counting*

Seven days before the surgery, retrograde labeling with a solution containing 2% fluorogold (FG; Fluorochrome, LLC, Denver, Colorado) and 1% 1,1′-dioctadecyl-3,3,3′,3′-tetramethylindocarbocyanine perchlorate (Di-I, 468495, Sigma-Aldrich, St. Louis, MO) was performed as described previously (Himori et al., 2013; Nakazawa et al., 2006). Briefly, the animal was anesthetized and the skin over the cranium was incised to expose the scalp. A hole of 1 mm in diameter was made on each side of the skull with a drill 4 mm posterior to the bregma and 1 mm lateral to the midline. One microliter of the FG or Di-I solution was slowly injected at a 2 mm depth from the surface of skull with a Hamilton syringe equipped with 32G needle. The overlying skin was sutured with 6-0 nylon, and antibiotic ointment was externally applied.

FG- or Di-I-labeled RGCs were counted at various survival times as described previously (Himori et al., 2013; Nakazawa et al., 2006) under fluorescence microscopy (Leica Microsystems, Wetzlar, Germany) using a UV or Rhodamine filter set. Briefly, the retinas were fixed in 4% paraformaldehyde (PFA) for 2 h. Retinas were then flat-mounted onto glass slides, and RGCs labeled with FG or Di-I were counted in 12 distinct areas of 2.46×10^{-2} mm^2 each (three areas per retinal quadrant at 1/6, 3/6 and 5/6 of the retinal radius). The density of the RGCs was defined as an average value of the 12 fields. The counting was performed by two independent investigators in a masked fashion and the data were averaged. To count surviving RGCs after NC or the induction of OH, the retinas were harvested 7 days after NC or 30 days after OH induction.

4.3. *Surgical procedures for optic nerve crush, ocular hypertension induction, and excitotoxicity*

Seven days after retrograde labeling, an NC procedure (Himori et al., 2013; Yasuda et al., 2014) or the induction of OH were performed as described in our previous reports (Nakazawa et al., 2006). For NC, the optic nerve was exposed, crushed with fine forceps for 10 s and released. Blood circulation was then confirmed to be normal and antibiotic ointment was applied. To investigate the role of KA receptors in the RGCs of the NC eyes, MK801 or CNQX (Sigma) were administered intraperitoneally. To induce OH, the right pupil was dilated with a topically applied mixture of phenylephrine (5.0%) and tropicamide (0.8%) 10 min prior to laser irradiation. The anterior chamber was flattened by the removal of aqueous fluid, and laser photocoagulation of the limbus was performed with a 200 μm spot size and 100 mW laser power for 0.1 s. The laser beam was directly focused on the corneal limbus with 100±10 (mean±S.D.) confluent spots. After treatment, 0.1% atropine and an antibiotic ointment were administered to the cornea. IOP was measured weekly with applanation tonometry, as described previously (Matsubara et al., 2006), in both eyes over a 4-week period after laser irradiation. We excluded mice from the experimental group if their first measurement of IOP was not 30% above the baseline. Excitotoxicity was induced with the intravitreal administration of KA (0.1, 1, 10 nmol/eye) (Nakazawa et al., 2006; Nakazawa et al., 2008). Seven days after the administration of KA, the retinas were flat mounted and surviving FG-labeled RGCs were counted.

4.4. *Histological axon counting*

All quantitative analyses included at least 3 sections from each of 8 mice for each experimental condition. After extraction, the